Beam Lithography, Pattern Formation, and Nanowires

Mater. Res. Soc. Symp. Proc. Vol. 1181 © 2009 Materials Research Society 1181-DD01-04

Localized $^{56}Fe^{+}$ Ion Implantation of TiO_2 Using Anodic Porous Alumina

J. Jensen[1], R. Sanz[2], M. Jaafar[2], M. Hernández-Vélez[2,3], A. Asenjo[2], A. Hallén[4], M. Vázquez[1]

[1]Thin Film Physics Division, IFM, Linköping University, SE-581 83 Linköping, Sweden
[2]Instituto de Ciencia de Materiales de Madrid, CSIC, 28043 Madrid, Spain
[3]Applied Physics Department, Universidad Autónoma de Madrid, 28043 Madrid, Spain
[4] ICT-MAP, Royal Institute of Technology, SE-164 40 Stockholm, Sweden

ABSTRACT

We present result following localized ion implantation of rutile titanium dioxide (TiO_2) using anodic porous alumina as a mask. The implantation were performed with 100 keV $^{56}Fe^{+}$ ions using a fluence of $1.3 \cdot 10^{16}$ ions/cm^2. The surface modifications where studied by means of SEM, AFM/MFM and XRD. A well-defined hexagonal pattern of modified material in the near surface structure is observed. Local examination of the implanted areas revealed no clear magnetic signal. However, a variation in mechanical and electrostatic behavior between implanted and non-implanted zones is inferred from the variation in AFM signals.

INTRODUCTION

Regular nano- and micro-patterns have potential technological application in *e.g.* data storage, biological sensors or photonic crystals. Ion implantation is an ideal instrument to modify material properties in a controlled way [1], and very suitable for fabrication and tailoring of functional properties such as optical/magnetic patterns, nanoporous material and catalyst surfaces. An important issue is to control the specific implantation areas. The spatial controls of areas where the material changes take place are fundamental in order to develop functional devices or study collective responses. One way of creating regular structures, or an array of modulated physical properties, is with focused ion beam implantation (FIB). However, since currently only a few ion sources and restricted energies are available, the application of this method is limited. Another method is using ion beam-based projection methods, where the ion impact is restricted by a mask or template, enabling a parallel formation of well-ordered and localized material modification yielding structures with well-defined features and interesting material properties [2-4]. A special type of implantation mask, which within the last few years has received much attention, is anodic porous alumina membranes, which contain self-ordered nanopores. Until now only few studies have been performed with this mask for ion beam nanolithography using keV ions [5,6,7].

Titanium dioxide (TiO_2) is a particularly versatile material with extensive technological application. Implanting this material with ferromagnetic ions makes it possible to obtain a diluted magnetic semiconductor [8], to be applied in future spintronics devices. Here one wants to avoid the clustering of doped species. However, for other application like magnetooptics, magneto-transport, and nanomagnetism the system must be composed of nanoclusters dispersed in a semiconductor or dielectric matrices [1]. Previous results on continuum implanted TiO_2 using 100 keV Fe ions [9] with fluences from $2 \cdot 10^{16}$ to $1 \cdot 10^{17}$ cm^2 showed the precipitation of metastable compounds such as $FeTi_2O_5$. More recently 180 keV Fe implanted rutile TiO_2 [10] was studied, presenting the precipitation and thermal evolution of epitaxial Fe and $FeTiO_3$

nanoclusters paying attention to their magnetic properties. In addition to interesting magnetic properties, doped TiO_2 is an extensively studied photo-catalytic semiconductor [11]. Doping of TiO_2 with Fe has been shown to enhance the efficiency of its photoactivity [12]. Even the optical properties of TiO_2 can be modified by ion irradiation [13].

In this work we present first results following localized ion implantation of rutile TiO_2 single crystal using 100 keV $^{56}Fe^+$ ions. The localized ion implantation was accomplished by irradiating the substrate through an anodic porous alumina membrane.

EXPERIMENTAL

Rutile single crystals (MTI Coorporation) with a <110> surface orientation were used as substrates (ρ=4.25 g cm^{-3}). The employed mask where 2 µm thick anodic porous alumina membrane (PAM) with 265 nm diameter and 450 nm lattice parameter, see Figure 1(a), obtained by a double anodization methods described elsewhere [14]. Prior to implantation the mask were placed on the substrate surface.

The samples were implanted with 100 keV $^{56}Fe^+$ ions at room temperature to a total fluence of $1.3 \cdot 10^{16}$ ions/cm^2. The average scanned ion beam flux was kept constant at about $7 \cdot 10^{11}$ cm^{-2} s^{-1}. Simulations of the implantation profiles was carried out by the TRIM (version SRIM2008) code [15], suggesting a near Gaussian ion distribution with a projected range of 50 nm and a straggling of 20 nm.

As the aspect ratio of the pores in the mask is small, giving an acceptance angle of approximately 5°, no alignment procedure was employed [16] and the irradiation was thus done at normal incidence. According to the TRIM code, the 100 keV Fe ions are completely stopped by the 2 µm thick PAM material (ρ= 2.3 g cm^{-3} [16]), so substrate areas between the pores should not be exposed directly to the ion beam. The lateral projected range and straggling is estimated much smaller than the average pore distance, so there should be no overlap of implanted volumes and essential no damage between the pores. Consequently, the exposed areas of the substrates under the masks roughly correspond to 54 percent of the total area. The maximum peak concentration of Fe located within the implanted volumes is ≈3.0%, given by TRIM simulation.

After implantation the PAM was removed by immersing in deonized water followed by a cleaning process with acetone using an ultrasonic bath. A LEO 1550 FEG high-resolution scanning electron microscope (SEM) was used to investigate the surface morphology. The samples implanted through PAM were furthermore investigated by atomic force microscopy (AFM) and magnetic force microscopy (MFM). The AFM/MFM measurements were carried out in dynamic mode using a Cervantes model from Nanotec. We used commercial Nanosensor PPP-MFMR probes. Finally, structural analysis of the substrate was performed by means of grazing incidence (3°) X-ray diffraction measurements using Cu, $K_{\alpha 1}$ (1.5604 Å) radiation and elemental analysis was performed by energy dispersive X-ray spectroscopy (EDS).

RESULTS AND DISCUSSION

The SEM observations of the irradiated sample show a clear contrast between implanted (damaged) and non-implanted areas, see Figure 1(b). The image shows an array of implanted zones in a hexagonal arrangement formed through the 'patterned' ion implantation. The sizes of

the implanted zones are similar to the mask pore holes with no appreciable change in the shape or size of implanted areas compared to original mask features. The ion implantation through the PAM thus yields a replication of the mask features and well-defined pattern to the substrate surface using the present ion energy and fluence. Note the interesting contrast seen at the border between implanted and virgin surface area.

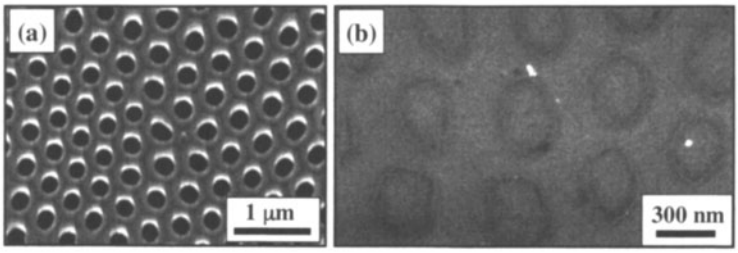

Figure 1. Scanning electron micrographs of (a) an anodic porous alumina membrane (PAM), the employed mask, and (b) the <110> rutile TiO_2 surface after ion implantation through such a mask with 100 keV $^{56}Fe^+$ to a fluence of $1.3 \cdot 10^{16}$ ions/cm^2. The mask was removed and the substrate cleaned before observation.

In order to check the existence of contaminations from the mask on the surface, EDS measurements were carried out. The EDS measurements showed an atomic composition of Ti and O in stoichiometric proportions. Even though Fe is detected, the total amount could not be exactly determined. The implanted Fe leads only to a small characteristic X-ray peak, which is residing on a large continuum background in the X-ray spectrum from the substrate. No traces from atomic species present in the PAM (Al and P) were detected, within the detection limit. Interesting is to note that even in an optical microscope a regular variation in optical reflectance was seen. This indicates a localized modification of the optical properties. Changes in optical absorbance of rutile have been observed after implantation with 64 keV Ni^+ ions [17].

To investigate the change in surface morphology after 'patterned' ion implantation, AFM measurements were performed, see Figure 2. A contrast, seen as a depth variation, is clearly observed. Non-implanted areas did not present any remarkable change of the surface morphology, having a maximum RMS roughness value of 0.69 nm. Implanted zones exhibit a crater shape with a convex structure inside with an average height of 2.5 nm from the bottom of the crater. A detailed profile of one of the structures is presented in Figure 2(b). The contrast seen by SEM in the implanted areas in Figure 1(b) is believed to be related to the depth profile observed by the AFM measurements.

The depression in the structures may originate by a combined effect of sputter erosion and a change in density caused by the induced ion damage. A simple TRIM simulation (for amorphous TiO_2) yields a sputter depth up to 6 nm for the applied fluence. However, the convex structure obtained in samples irradiated through the PAM, can be ascribed to the restricted implantation where other effects such as redeposition of sputtered material could be more noticeable than in not masked conventional implantations. Also, sputtering of mask material is possible although no trace of deposited mask material were detected.

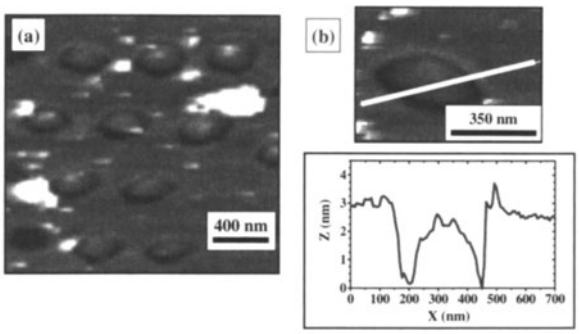

Figure 2. (a) AFM image of the rutile surface after implantations through a PAM mask with 100 keV Fe ions to fluence of $1.3 \cdot 10^{16}$ ions/cm^2. (b) The profile of an AFM line scan through an exposed area. The mask was removed and the substrate cleaned before observation.

The local magnetic behavior of the localized implanted samples was measured by MFM. In Figure 3 we present the topographic (a) and frequency shift images (b and c). Image contrast associated to a frequency shift, measured at the same tip-sample distance as the topography, resulted in a maximum value of 4 Hz. The origin of this variation can be ascribed to electrostatic interaction or changes in the mechanical properties such as visco-elasticity, adhesion and/or friction of the implanted areas. The contrast may even arise due to changes in dielectric properties [18]. This phenomenon of frequency shift has not been studied in detail at the present moment. But a local change in dielectric property may be explained as a combination of a change in the active surface chemistry of TiO_2 [19] and the effect of the defects originated by ion implantation. Another source for changes in the dielectric property is the existence of small Fe metal clusters surrounded by a dielectric material. To study the magnetic signal a second pass, where the tip- sample distance was increased to about 25 nm, was performed. We did not see any clear magnetic contrast from implanted and non-implanted areas, Figure 3(c). Observation of no magnetic contrast can originate by the low magnetic moment in the implanted zones, being lower than the detection threshold of the instrument.

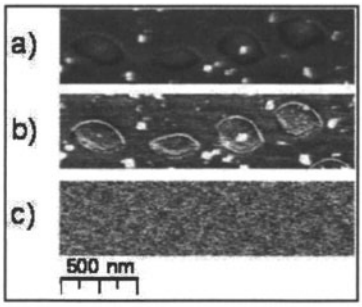

Figure 3. AFM and MFM images showing (a) topographic signal, (b) frequency shift, and (c) frequency shift at 25 nm from the surface of a rutile substrate after implantation with 100 keV $^{56}Fe^+$ ions to a fluence of 1.3×10^{16} ions/cm^2 through a PAM.

Preliminary grazing incidence XRD measurements of the rutile substrate implanted with 100 keV $^{56}Fe^{+}$ ions, without the use of a mask (i.e. continuum implantation), is shown in Figure 4. The peaks seen in the virgin substrate are gone. However, in addition to an amorphous halo, broad peaks belonging to new phases are observed. The peaks are situated close to the positions of diverse Fe oxides and Fe-Ti compounds. However, taking into account the reported existence of metastable Fe-Ti precipitates generated by ion implantation processes [9] it is not possible to precisely assign the detected peaks by just relying on the XRD technique. The existence of metastable precipitates may justify the observed changes in dielectric properties. It can also explain the missing magnetic contrast, as seen by MFM, due to a superparamagnetism behavior of those precipitates or just a low magnetic moment.

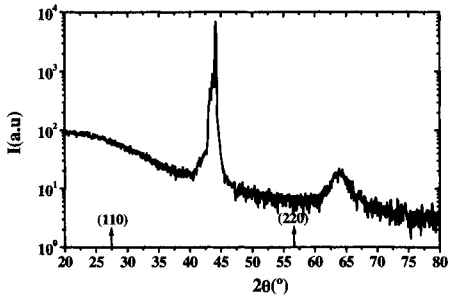

Figure 4. Grazing incidence XRD diffractogram of a <110> rutile substrate after continuum implantation with 100 keV $^{56}Fe^{+}$ ions to a fluence of $1.3x10^{16}$ ions/cm^2. The angle of incidence for GIXRD was 3°. The original rutile diffractions peak positions (110) and (220) are indicated with arrows.

In a recent study, where we implanted ZnO with 35 keV $^{55}Mn^{+}$ ions, we saw different results in samples implanted through PAM as compared to samples implanted over the whole surface (continuum implantations) [20]. The differences manifested themselves by *e.g.* dissimilar XRD spectra and magnetic response as observed by SQUID. In addition, it has previously been observed that localized ion implantation within micrometer size areas may lead to different diffusion and clustering properties as compare to continuum implantation as observed after Au ion implantation into TiO_2 [21,22]. It is thus suggestive that also in the present case of sub-micrometer restricted implantation, there might be differences in continuum and masked implantation and that the XRD data shown in Figure 4 are not representative for the masked implantation.

CONCLUSIONS AND OUTLOOK

Applying a PAM as stencil mask, localized zones have been successfully implanted, with an acceptable accuracy of pattern reproduction. The present stencil mask may therefore be used for creating well defined material contrast employing ion beam implantation techniques. The detected changes in local dielectric properties in the restricted implanted samples deserve a more carefully study due to the interesting applications of the active surface chemistry of TiO_2 and its optical properties.

There was no detectable magnetic response of restricted implanted zones as observed by MFM. However, it is not possible to rule out a ferromagnetic response referring to reported

results obtained under continuum ion implantation conditions. Taking into account the possibility for an existence weak ferromagnetic signal, other techniques, *e.g.* X-ray magnetic circular dichroism, should be employed to study this possibility in detail. These studies are currently in progress.

Nonetheless, localized ion implantation may lead to different diffusion and clustering properties as compare to continuum implantation, which need to be look into. This may have interesting consequences for magnetic, optical and surface chemical surface properties when performing restricted ion implantation.

ACKNOWLEDGMENTS

This work was supported in part by the Spanish Ministry of Education under Grant MAT2007-6042. J. Jensen thanks the Carl Tryggers Foundation and Linköping University through the VR Linneaus grant LiLi-NFM for financial support. M.J. Thanks the CAM for the financial support.

REFERENCES

1. A. Meldrum, R. F. Haglund, Jr., L. A. Boatner, and C. W. White. Adv. Mater. **13**, 1431 (2001).
2. T. Shibata, K. Suguro, K. Sugihara; T. Nishishashi; J. Fujiyama; Y. Sakurada, IEEE transactions on semiconductor manufacturing **15**, 183, (2002).
3. E. Knystautas, '*Engineering Thin Films and Nanostructures with Ion Beams*', Optical Science and Engineering Series Vol. **95** CRC Press (2005).
4. *Ion-beam-based Nanofabrication*, edited by D. Ila, J. Baglin, N. Kishimoto, P.K. Chu, MRS symposium proc. Vol **1020** (2007), and MRS spring meeting 2009, symposium DD.
5. N. Matsuura *et al.*, Appl. Phys. Lett. **81**, 4826 (2002).
6. S.W. Shin *et al.*, Nanotechnology **16**, 1392 (2005).
7. M. Nakamura, S. Nigo, N. Kishimoto, Trans. Mater. Res. Soc. Jpn. **33**, 1101 (2008).
8. R. Janisch, P. Gopal, and N. A Spaldin. J. Phys.: Condens. Matter **17**, R657 (2005).
9. M. Guermazi *et al.*, Mat. Res. Bull. **18**, 529 (1983)
10. M. Zhou *et al.*, J. Appl. Phys. **103**, 083907 (2008).
11. A. Fujishima, K. Hashimoto, and T. Watanabe, *TiO_2 Photocatalysis: Fundaments and Applications*, BKC, Tokio, (1999).
12. C. Adán, A. Bahamonde, M. Fernández-García, A. Martínez-Arias, Appl. Catal. B **72,** 11 (2007).
13. J. Jensen, M. Skupinski, K. Hjort, R. Sanz, Nucl. Instrum. and Methods B **266**, 3113 (2008).
14. H. Masuda and F. Fukuda, Science **268**, 1466 (1995).
15. www.srim.org.
16. R. Sanz, J. Jensen, A. Johansson, M. Skupinski, G. Possnert, M. Boman, M. Hernandez-Vélez, M. Vazquez, K. Hjort. Nanotechnology **18**, 305303 (2007).
17. S. Zhu, L.M. Wang, X.T. Zu, and X. Xiang, Appl. Phys. Lett. **88**, 043107 (2006).
18. C. Dumas *et al.*, Microelectronic Engineering **85**, 2358 (2008).
19. U. Diebold, Surf. Sci. Rep. **48**, 53 (2003).
20. R. Sanz, J. Jensen, G. González-Díaz, O. Martínez, M. Vázquez and M. Hernández-Vélez, Nanoscale Research. Lett., Accepted (2009).
21. K. Sun, S. Zhu, R. Fromknecht, G. Linker, L.M. Wang, Materials Letters **58**, 547 (2004).
22. R. Fromknecht, G. Linker, L.M. Wang, S. Zhu, K. Sun, A. van Veen, M. van Huis, J. Niemeyer, T. Weimann, J. Wang, Surf. Interface Anal. **36**, 193 (2004).

Mater. Res. Soc. Symp. Proc. Vol. 1181 © 2009 Materials Research Society 1181-DD13-13

Importance of internal ion beam parameters on the self-organized pattern formation with low-energy broad beam ion sources

Marina I. Cornejo, Bashkim Ziberi, Michael Tartz, Horst Neumann, Frank Frost, Bernd Rauschenbach

Leibniz-Institut für Oberflächenmodifizierung e.V. (IOM) Permoserstr. 15, D-04318 Leipzig, Germany

E-mail: marina.cornejo@iom-leipzig.de

ABSTRACT

A first qualitative approach to the importance of the divergence angle and angular distribution of the ions within the broad beam (here called internal beam parameters) on the pattern formation by low-energy ion beam erosion is presented. Si (100) surfaces were irradiated with Kr^+, with an ion energy of 2 keV, using a Kaufman type broad beam ion source. It is found that the operating parameters of the broad beam ion source which are responsible for the angular distribution of the ions also affect the pattern formation. Especially, the effect of the acceleration voltage, discharge voltage, grid distance and operation time on the transition from ripple to dot pattern with increasing ion beam incidence angle were analyzed. The results represent additional evidence about the significance of the internal beam parameters and the need of the further investigation of their role on the pattern formation by low-energy erosion.

INTRODUCTION

The low-energy noble gas ion beam erosion of solid surfaces is a simple bottom-up approach for the generation of nanostructures. For certain sputtering conditions well ordered self-organized nanostructures (e.g., ripples, dots) can be formed. Due to the use of broad beam ion sources, low-energy ion beam erosion is particularly suitable as a cost-efficient method to produce large-area nanostructured surfaces in a one-step process.

The surface topography evolution is, in general, attributed to the competition of curvature dependant sputtering that roughens the surface and smoothing by different surface relaxation mechanisms [1-5]. It is also well known that the incidence angle of the ions is a critical parameter that determines the surface topography. On Si surfaces, different topographies emerge on the surface due to the bombardment (without rotation of the sample) at different ion beam incidence angles [6]. Ion beam incidence angle refers here to the angle between the substrate normal and the ion source axis (geometrically defined incidence angle). Inherent to all broad beam ion sources, which are essential for large area processing and often used for low-energy ion beam erosion, the ion beam exhibits a certain divergence, i.e. the ion trajectories are not strictly parallel to each other. This generates a spread of the local incidence angles with respect to the geometrically defined ion beam incidence angle. There are only few works about the patterning by low-energy ion beam erosion where the angular distribution was contemplated and considered important for the surface topography evolution [7, 8]. There could be a connection between the variety of results obtained by the different research groups [9-12] and the divergence angle and angular distribution of the ions, here called internal ion beam parameters.

In this work the effect of some operational parameters of a broad beam Kaufman type ion source on the surface topography evolution is presented. Among all the experimental parameters that affect the pattern formation by low-energy ion beam erosion here the focus was set on the influence of those that affect the internal ion beam parameters. First, the effect of the accelerator voltage, i.e. the voltage applied to the accelerator grid is shown. Additionally, the importance of the discharge voltage, valid for Kaufman type broad beam ion sources, was analyzed. The geometry of the extraction system is also known to affect the ion angular distribution. In this regard the effect of the distance between the extraction grids and the effect of the grid alteration with the time on the surface topography are presented.

EXPERIMENTAL DETAILS

The ion source used for the experiments is a home-built Kaufman-type broad beam ion source (beam diameter 180 mm) equipped with a two-grid multi-aperture ion optic system. The first grid (screen grid) is at floating potential. The positive beam potential is applied to the plasma anode. The second grid (accelerator grid) is at a negative potential with respect to the grounded chamber and sample stage. The total voltage of the beam is the sum of the voltages applied to both grids. The overall ion beam parameters as the divergence angle and the angular distribution of the ions within the beam are determined by the full set of ion source parameters: grid voltages, plasma parameters and their spatial distribution and grid geometry [13, 14]. The energy of the ions on the target, however, depends only on the potential difference between the plasma and the target (usually at ground) and is defined here by the beam voltage. More details about the broad beam ion source used are given elsewhere [15].

The samples used were commercially available epi-polished (100) Si substrate (*p* type and 0.01 and 0.02 Ω cm) with a root-mean-square (rms) roughness of ~0.2 nm. The samples were mounted on a water cooling (temperature approx. 285 K) substrate holder in a high vacuum chamber with a base pressure of 1×10^{-6} mbar. The ion beam incidence angle (α_{ion}) can be varied from 0° and 90° in steps of five degrees. An additional angle adjustment is achieved using a sample holder with facets of one degree. The samples were irradiated with Kr^+ ions with a kinetic energy (E_{ion}) of 2 keV and a fluence (Φ) of 6.7×10^{18} cm^{-2}. The acceleration voltage (U_{acc}) and discharge voltage (U_{dis}) were varied from -200 to -1000 V and 50 to 150 V respectively. The distance between the two grids (d) was changed from 1 mm to 2 mm in some of the experiments in order to analyze the influence of this parameter. The surface topography was analyzed by scanning force microscopy (AFM) using a Dimension 3000 system with Nanoscope IIIa controller from Digital Instruments operating in TappingMode™. The AFM results presented have a resolution of 512 × 512 pixels, and Si probes with (nominal) tip radii smaller than 10 nm were used.

RESULTS AND DISCUSSION

In Fig. 1 AFM images of different topographies emerging on Si surfaces when irradiated at different ion beam incidence angles without sample rotation are presented. It is shown that increasing the ion beam incidence angle from 15 to 30°, the transition from ripples to smooth surface takes place. An intermediate transition structure (here called transition structure ripples-dots) is clearly observed (Fig. 1b). The ripples begin to transform into dots ordered along the previously existing ripples, as shown here for E_{ion}= 2 keV and U_{acc}= -1000 V.